



Multi-layer continuum model for adhesive FM 300-2 in end-notched flexure carbon laminate

O. Rodera^{*}, N. Pournoori, P. Hakala, M. Kanerva, J. Jokinen

Tampere University, Faculty of Engineering and Natural Sciences, 33100, Tampere, Finland

ARTICLE INFO

Keywords:

Toughened adhesives
Composites
Finite element analysis
Delamination

ABSTRACT

The current investigation analyses the un-stable crack initiation of an adhesively bonded End Notched Flexure (ENF) specimen by means of a continuum damage formulation, based on the Bazant's crack model, to reproduce accurately the load response and the fracture process zone of the adhesive. The specimen consisted of carbon fibre reinforced polymer adherends and two sheets of FM 300-2 adhesive films. The need of this implementation arose from experimental observations of normal transverse damage mechanisms at the bondline during the crack initiation. The damage model was based on a multi-layer configuration of the adhesive meso-structure that accounted for two damage activation functions in the normal and shear transverse directions. The results demonstrated the capability of the model to predict closely the force drop in the load–displacement curve of the ENF test. Different multi-layer configurations were studied following proper meso-structure simplification of the adhesive to use elastic and damage-capable layers in a correct order and thicknesses. The rise of the modelled shear strength allowed for keeping enough stored strain energy contributed to the low triaxiality stress in the bondline. Finally, the results demonstrated a significant influence of the layers modelling the knitted carrier to the local mechanisms of tensile fracture because of the normal transverse deformations. Unclassified. Based on Foreground information under EDA Contract No B.PRJ.RT.670 covering the Ad Hoc Project entitled "PATCHBOND II".

1. Introduction

The modelling of adhesive bonded joints requires reliable methods of failure prediction. Different approaches have been developed by the scientific community based on the fracture and continuum mechanics. Many of the methods have used strength-based criteria and focused on the initial failure or pre-crack growth with a minor representation of the Fracture Process Zone (FPZ). For the characterization of adhesives with metallic and Carbon Fibre Reinforced Polymer (CFRP) adherends, the Mode I fractures have been tested by using Double Cantilever Beam (DCB). While, for the Mode II testing, the three point bending test using the End Notched Flexure (ENF) specimen is probably the most popular method. The typical bond–slip curve has been modelled with parameters of peak shear traction and a critical strain energy release rate. However, as stated by numerous investigations [1–3], the response of the adhesive is not only influenced by the shear damage mechanisms, but also by relative normal transverse mechanisms perpendicular to the bondline. These opening deformations have been reported to cause unstable load response indicated the force drop, typical of ENF tests [2, 4–6]. A work by Leone et al. [1] reported a type of ENF test to prevent the Mode I appearing in the crack by applying clamps to the test. The

results of the clamped tests revealed 30% higher fracture toughness than in the traditional ENF test.

To avoid un-stable crack propagation, the Four-Point End Notched Flexure (4ENF) test has been studied as a method for Mode II. Leal and Campilho [7] implemented a Cohesive Zone Model (CZM) to evaluate shear toughness in adhesive joints through ENF and 4ENF tests. These numerical simulations assessed the accuracy and efficiency of these methods, showing their potential for estimating fracture toughness in adhesive applications. Recently, Li and Lubineau [8] explored methods to improve ENF test (the crack growth) stability, identifying challenges with the instability and proposing modifications, such as adjustments in specimen geometry or loading conditions. Oshima S. et al. [9] revealed that, under Mode II loading, macroscopic crack growth occurred due to the coalescing of microcracks in adhesively bonded CFRP joints.

Formulations with CZM for structural adhesives have been applied to reproduce the fracture response in joints. Turon et al. [10] proposed a constraint for the pure-mode strength parameters and fracture toughness, and a parameter for the penalty stiffnesses ensuring proper energy dissipation under mixed-mode loading. Based on this, Sarrado et al. [11] developed a finite-thickness CZM with overall dependency

^{*} Corresponding author.

E-mail address: oscar.roderagarcia@tuni.fi (O. Rodera).

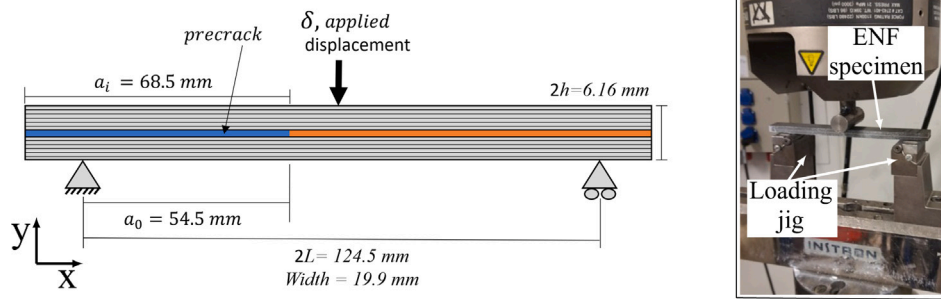


Fig. 1. Measurements and set-up of the ENF mechanical testing, and the coordinate system of test system.

on only material and fracture properties. For that, displacement of the bulk part material field was de-coupled from the interface displacement in order to fulfil the Turon's constraint and define the real thickness in the model.

The CZM formulations provide a good ratio between computational efficiency and accuracy in reproducing the response of structure. However, this method has a shortcoming in the prediction of unconstrained localization of damage along the FPZ size — thickness. This eventually limit the reproduction of local failure mechanisms, especially with the meso-structure films subjected to un-stable conditions. The predictions of high-resolution, local damage mechanisms and FPZ are beyond typical CZM applications of joints in finite element basis, i.e., single cohesive element thickness or zero-thickness at bondline.

An alternative to CZM is the Continuum Damage Model (CDM) with the ability to reproduce precisely size of FPZ. With CDM, activation of suitable failure functions can be assigned to failure mechanisms and local stiffness degradation always occurs for correct dimension (thickness). De Moura et al. [12] used two different methods to simulate damage propagation of bonded joints tested in pure Modes I and II. Their CDM was based on a trapezoidal traction–separation law to account for the ductile behaviour of the adhesive and was applied to reproduce DCB and ENF-type of loading. The cohesive parameters were determined by using an inverse method applied to the test results. Their reported results presented the maximum force; however, no experimental comparisons were provided in the publication. De Moura et al. analysed the mesh sensitivity along with evolution of stiffness, where it was not able to reproduce accurately the typical non-linear response. In a recent work, Rodera et al. [13] reproduced the experimental response of an adhesive subjected to Mode I fracture test and developed a non-local constitutive damage model. In particular, they used CDM and multi-layer configurations to consider the internal carrier supporting the resin part in actual adhesive product. In their work, strength and fracture properties were experimentally determined and the multi-layer modelling predicted failure occurring close to the adhesive-adherend interface.

In the current work, a CDM formulation is developed to reproduce accurately the un-stable crack initiation under shear loading, i.e. testing via ENF method. CFRP adherends of the specimen are bonded using especial adhesive film (sheet) including a knitted carrier. Experimental observation show diagonal cracks at the adhesive FPZ — revealing the existence of opening deformations. The meso-structure of the adhesive model is defined by a multi-layer approach. In this approach, the knitted carrier is simplified by an elastic layer with fitted thickness, while the matrix phase is degraded by proper dissipation in a brittle response. The force drop in the specimen response is accurately predicted correlating with the definition of the shear strength parameter. The model enables properly stored strain energy during the force drop process, and had a low triaxiality stress profile along the bondline. Additionally, the results demonstrated significant influence of the knitted carrier layer affecting local mechanisms of tensile fracture as a consequence of normal transverse deformations. The added implementations of Virtual Crack Closure Technique (VCCT) and CZM for interlaminar delamination enabled the potential to CFRP failure.

2. Materials and methods

2.1. ENF specimen preparation and testing

The ENF specimens were manufactured using CFRP laminates and adhesive film sheets. The laminates consisted of 20 AS4/3501-6 Unidirectional (UD) plies, stacked in a sequence of $[0/0/0/-45/-45/0/0/45/-45/0]_{SE}$. This primarily represents quasi-isotropic behavior, offering improved tensile strength and increased bending stiffness under ENF flexure. This enhancement was achieved by replacing each 90° ply adjacent to a 45° ply in the original lay-up with a 0° ply, optimizing the structural performance. In addition, a 0° ply at each side of the adherend was included in order to have $0^\circ-0^\circ$ interface at the central part of the joint. Prior to curing, the adherends were sanded with 180 grit sanding paper until fibres appeared on the first ply. The adhesive material for this study was adhesive film FM 300-2 (Solvay) in the form of sheet with a 0.36 mm nominal thickness [14]. This adhesive type is a 121°C curing modified epoxy film with a knitted polyester carrier. Two adhesive sheets were placed at the bondline (nominal crack thickness of 0.56 mm). The release film (20 μm thickness) was placed between the adhesive films in order to create a pre-existing crack at the location of 68.5 mm (i.e. 54.5 mm when standard delamination length is measured, a_0 [15]). The CFRP laminates were bonded immediately after receiving a surface treatment based on: removal of the peel ply, hand sanding until first ply and a final dry wiping step [16]. The joint was cured under vacuum of 0.7 bar by using the air-circulating oven (TS 8136, Termaks). The individual test specimen was cut by using water jet cutting. In total, six specimens were manufactured with a mean length of 152.5 mm and a mean width of 19.9 mm and a total thickness of 6.2 mm (see Fig. 1).

Flexural testing was conducted using the universal testing machine (8800, Instron) with a load capacity of 100 kN. The quasi-static tests were conducted under the displacement control with a displacement rate of 2 mm/min. The displacement was applied up to 12 mm before the unloading in those specimens that showed un-stable crack growth.

Digital Image Correlation (DIC) technique (StrainMaster, LaVision) was used to study the specimen deformations and initial length of the pre-crack. DIC is a method to compute full-field deformation with specific algorithms applied to image data [17]. For visualization of crack evolving, a low-speed optical camera (StrainMaster Compact, LaVision, Germany) was used to record the specimen during testing.

2.2. Model of the adhesive forming the bondline

The numerical approach in this work is based on the CDM implementation into layers representing the polymer matrix component. The analysis of the mixed-mode fracture along with the FPZ (at between the two adhesive sheets) was also carried out by using the VCCT and CZM methods for comparison. Potential delamination in the CFRP laminate was simulated at the first upper interface ($0^\circ-0^\circ$ interface) of the upper adherend by using only the CZM.

The reasoning for the multi-layer configuration is shown in Fig. 2. The complex and partly random geometry of the knitted carrier (two

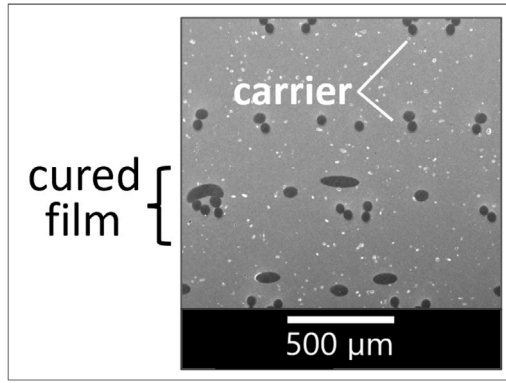


Fig. 2. Electron microscopy cross-section imaging of the cured film-adhesive as a pure-adhesive specimen.

Table 1
Elastic properties of the adherends and adhesive in this study [1,14,19,20].

UD ply		Film adhesive			
E_{11} :	140 (13.21) GPa	G_{12} :	5.17 (3.55) GPa	E_m :	2.45 GPa
$E_{22} = E_{33}$:	10 (13.21) GPa	G_{13} :	5.17 (8.97) GPa	ν_m :	0.38
$\nu_{12} = \nu_{13}, \nu_{23}$:	0.3, 0.53	G_{23} :	2.9 (3.55) GPa	G_m :	0.89 GPa

sheets) is here compressed into a solid elastic layer. Fig. 2 presents a part of the cross-section of a cured adhesive specimen with multi films stacked up from a previous work [13].

Fig. 3-A shows the three alternative CDM configurations studied here for the adhesive meso-structure — single and multi-layer (CMC and MCM) models with polymer matrix (M) and carrier (C). These allow for studying precise damage mechanisms at the bondline. The multi-layer model follows the adhesive structure consisting of carrier (textile) in the real adhesive film that is homogenized as a continuum solid layer. The behaviour in the carrier is assumed linear-elastic. The matrix layer is defined with an elastic-brittle response through CDM. The application of CZM and VCCT at ply-ply interface, as well as their comparative analysis for adhesive performance, is also presented.

Fig. 3-B presents the schematic representation of the adhesive response characterized by the shear transverse deformation as a consequence of the sliding, and a coupled mechanism due to transverse deformations in the normal direction to the bondline (i.e. opening and compression). The predictions regarding failure initiation in these performances enable the modeling of diagonal cracks at the layer level through the formulation of a specialized directional damage variable. Published experimental data from carbon-composite ENF tests [1,3] with adhesives revealed the potential occurrence of diagonal cracks associated with transverse normal deformations relative to the bondline. Similar observations were also found at the thicker zones of the interlaminar in glass and carbon fibre reinforced laminates [18]. For that, the modelling of matrix degradation requires activation of two damage functions predicting failure initiation in appropriate directions; this can result in an anisotropic stiffness degradation by two damage variables.

Table 1 presents the experimentally confirmed elastic (orthotropic) properties of the CFRP ply and the FM 300-2 adhesive film sheet. The elastic constants of a ‘compressed’ carrier layer were set to be same as those of the film adhesive in total. The engineering constants (in between brackets) for the $\pm 45^\circ$ plies of the laminate lay-up but given in the specimen coordinate system (123) were calculated using the ESAComp (version 2020, Altair) [20]. Table 2 shows the fracture properties at the crack initiation stage used for the VCCT, CZM and adhesive continuum models. The values in between parentheses in CZM represent the properties for the bondline.

Table 2

Fracture properties for the methods used in this study. The values in between parentheses in CZM represent the properties for the bondline. Subindex c (except for X_c) refers to the critical values comparable to test results of fracture toughness.

VCCT (comparison) [21]	CZM (in CFRP & bondline)	CDM
G_{Ic} : 1820 J/m ²	r_n^0 : 35 MPa [22,23]	X_n : 35 MPa [13]
G_{IIc} : 6230 J/m ²	r_s^0 : 55 MPa ^{ab} [14]	X_c : 61 MPa [13]
$\alpha = \beta$: 0.68	G_{Ic} : 72 (1820) J/m ² [24]	S_I : 55 MPa ^{ab} [14]
	G_{IIc} : 779 (6230) J/m ² [24]	G_{nc} : 1820 J/m ² [21]
	$\alpha = \beta$: 0.71 (0.68) [24]	G_{shc} : 6230 J/m ² [21]

^a Subjected to sensitivity analysis in the current study.

^b Maximum stress from testing with contact extensometer KGR-1 (thick adherend lap shear test).

2.2.1. Analysis method for LEFM debond

The VCCT evaluates the energy release rate (ERR) using the separation of nodal points adjacent to the crack tip and the reaction force at the crack tip. The VCCT evaluates the momentary ERR by using the reaction force and the separations at the crack tip. The computation of the ERR can be obtained from the following equation [25,26]:

$$G_{II} = \frac{F \Delta u}{2B \Delta a} \quad (1)$$

where F is the reaction force at the crack tip, Δu is the separation of nodal points adjacent to the crack tip, B is the element width and Δa is the element length. The formulation is available in the commercial finite element software Abaqus [27]. The modelling of the LEFM interface was based on two solid elements representing each one, a homogenized adhesive sheet (see properties in Table 1); and a zero-thickness cohesive element at the bondline. The modeling of the LEFM interface was based on a zero-thickness cohesive element positioned at the bondline. Solid elements were used in between representing the two homogenized adhesive sheets (properties detailed in Table 1).

2.2.2. Cohesive zone model for comparison and delamination

The CZM of the commercial finite element (FE) software Abaqus [27] was implemented at the adhesive bondline and adherend ply-ply interface. The damage onset was defined using a quadratic stress criterion:

$$\left(\frac{\langle \tau_n \rangle}{\tau_n^0} \right)^2 + \left(\frac{\tau_s}{\tau_s^0} \right)^2 + \left(\frac{\tau_t}{\tau_t^0} \right)^2 = 1 \quad (2)$$

where τ_n , τ_s and τ_t represent the components (normal, shear) of the traction vector. The peak values (τ^0) for the normal traction, 35 MPa, and shear component, 55 MPa, were taken from a preliminary analysis [13,23]. The damage evolution was defined by the power law equation:

$$\left(\frac{G_I}{G_{Ic}} \right)^\alpha + \left(\frac{G_{II}}{G_{IIc}} \right)^\beta = 1 \quad (3)$$

where G_I and G_{II} represent the energy release rates related to the pure Modes I and II. Subindex c refers to the critical value of ERR that is comparable to the standard test results of fracture toughness (composite delamination, or adhesive in a joint). The bi-linear traction-separation law was used in the analysis. The modelling of the interface at bondline and composite laminates was based on a zero-thickness cohesive element. Two solid elements represented the homogenized adhesive sheets.

2.2.3. CDM formulation

The bondline model follows a formulation of continuum damage mechanics. The complementary free energy density is defined as [28]:

$$\psi = \psi^{e-d}(\epsilon^e, d_n, d_{sh}) = \left(\frac{1}{2E_m} \right) \left(\frac{\sigma_{11}^2 + \sigma_{22}^2 + \sigma_{33}^2}{(1-d_n)} \right) - \frac{\nu_m}{E_m} (\sigma_{11}\sigma_{22} + \sigma_{22}\sigma_{33} + \sigma_{33}\sigma_{11}) + \frac{1 + \nu_m}{E_m(1-d_{sh})} (\sigma_{12}^2 + \sigma_{13}^2 + \sigma_{23}^2) \quad (4)$$

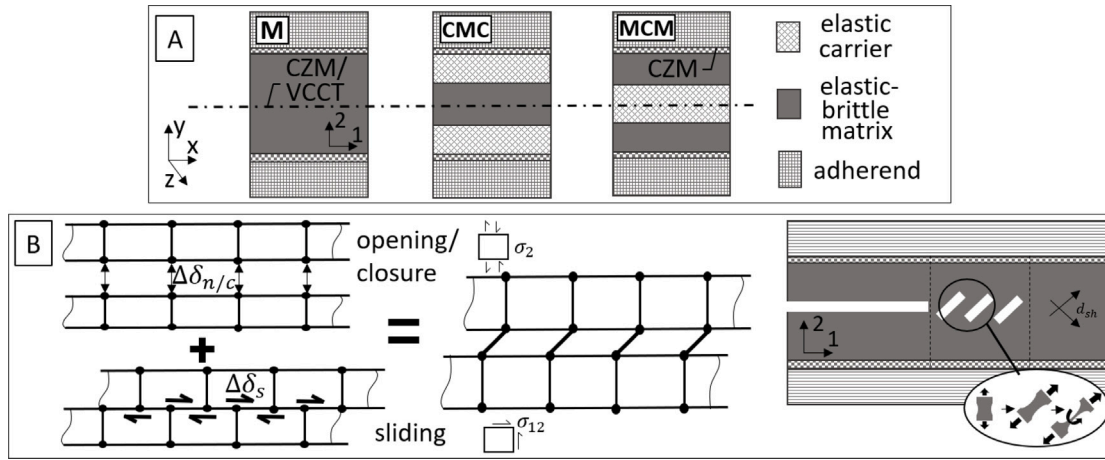


Fig. 3. (A) Conceptualization of adhesive failure model-including with single and layer configurations; (B) Representation of the failure mechanism during the local tensile (compressive) and shear deformations in the finite-thickness adhesive and the local ENF specimen's coordinate system (12(3)).

where E_m and ν_m are the Young's modulus and Poisson's ratio of adhesive (matrix phase). The d_n and d_{sh} are the damage variables corresponding to the tensile (and compressive) direction normal to the bondline, and the d_{sh} for the shear (transverse) direction; see the local specimen coordinate system in Fig. 3-B. σ_{ij} with $i, j = \{1, 2, 3\}$, is the stress tensor. Eq. (4) specifically requires defining the 123-coordinate system to align with the bondline whenever d_n and d_{sh} are separable. It is important to note that the model herein is developed for the bondline with layered meso-structure.

To ensure thermodynamically irreversible damage process, the dissipated energy by the external work supplier must not be negative, i.e., $\dot{\psi}^{e-d}(\epsilon^e, d_n, d_{sh}) - \dot{\sigma} : \epsilon \geq 0$. The compliance tensor can be found in Appendix A.

The current model encloses the elastic domain by two damage activation surfaces accounting for the tensile/compressive failure in normal direction and shear transverse mechanisms at the bondline. The surfaces are formulated by the damage activation function, F_n and F_{sh} ; $F_i(\phi_i, r_i) = \phi_i - r_i \leq 0$. The elastic domain threshold, r_i , is an internal variable of the constitutive model that relates the activation functions, F_i , with the damage evolution law.

The normal loading function, ϕ_n , that involves both the tensile and compressive responses, is formed by the criterion developed by Melro et al. [29], for brittle response in an epoxy-resin model. The criterion is based on a paraboloidal failure surface for 3D isotropic bodies [30].

$$\phi_n = \frac{3\bar{J}_2}{X_n X_c} + \frac{\bar{I}_1(X_c - X_n)}{X_n X_c} \quad (5)$$

where $\bar{J}_2 = 1/2 \bar{s} : \bar{s}$ is the second invariant of the deviatoric (effective) stress tensor. $\bar{I}_1 = \text{tr}(\bar{\sigma})$ is the first invariant. The effective stress tensor is calculated as $\bar{\sigma} = \mathbf{H}_0^{-1} : \epsilon$. \mathbf{H}_0 corresponds to the undamaged compliance tensor ($d_n = 0$). The X_n and X_c represent the normal tensile and compressive strengths, respectively, (whether or not stress state is normal or shear dominated).

The especial loading function involved with the shear failure is based on a plastic yield function adopted for composites under (transverse) shear loading by Sun and Chen [31]:

$$\phi_{sh} = \frac{\frac{3}{2}(\bar{\sigma}_2^2 + 2.2\bar{\sigma}_{12}^2)}{S_L^2} \quad (6)$$

where, $\bar{\sigma}_2$ and $\bar{\sigma}_{12}$ are the effective transverse stresses in normal and shear directions, respectively; The S_L parameter represents the shear strength of the adhesive layer, defined based on technical data provided by the manufacturer [14].

The inelastic numerical response is solved by using the Bazant's crack band model [32]. The energy dissipated per unit volume is regularized to ensure mesh objectivity via $g_i = \frac{G_i}{l^c}$ with $i = \{n, sh\}$.

G_n and G_{sh} are the fracture toughness in the normal and shear modes obtained from experimental tests. $l_{n,sh}^c$ is the characteristic element length.

The damage onset and evolution is expressed by the *Kuhn-Tucker* conditions. The damage evolution law is defined as an exponential function to represent the cohesive failure [29]:

$$d_i = 1 - \frac{e^{A_i(3-\sqrt{7+2r_i^2})}}{\sqrt{7+2r_i^2}-2} \quad \text{with } i = \{n, sh\} \quad (7)$$

The parameter A_i can be numerically calculated from the previous work of Rodera et al. [13]. The value of $l_{n,sh}^c$ was established as length of a line across for a first-order element in the harnessed model. To avoid a local snap-back effect in stress-strain response, the elastic energy of a FE at the localization must be lower or equal to the corresponding fracture toughness i.e. $l_n^c \leq \frac{2E_m G_n}{X_n^2}$ and $l_{sh}^c \leq \frac{2E_m G_{sh}}{S_L^2}$.

The consistent tangent stiffness operator was determined by the general form:

$$\mathbf{C}_m^T = \mathbf{C}_m + \mathbf{M}_m : \epsilon \quad (8)$$

where the \mathbf{C}_m is the damaged stiffness matrix and the tensor \mathbf{M}_m is defined in Appendix B.

2.3. FE models for ENF simulation

The FE modelling of the ENF specimen was performed by using Abaqus/Standard 2021. The specimen was modelled based on the plane strain state (2D with $\epsilon_{33} = 0$). The dimensions of the ENF model were 152.5 mm in length, 20 mm in width and 2.8 mm in thickness for each composite adherend. The boundary conditions (BC) consisted of two cylindrical pins at the lower adherend and one cylinder at the upper adherend with radiuses of 5 mm and 10 mm, respectively. The loading was based on applying a displacement (through thickness direction) to the upper cylinder, while the right and left bottom cylinders kept fixed. The distance between the fixed cylinders was 124.5 mm. A surface-to-surface contact between the cylinders and adherend surfaces were used with normal and tangent restriction. The pre-crack (frictionless contact) length was of 68 mm from left edge.

The mesh type was based on linear quadrilateral element with reduced integration (CPE4R). The enhanced hourglass control was opted. The total number of elements was of 49,790 with a length size of 0.10 mm (bondline) and 0.14 mm (laminate) in the thickness direction. Three elements per layer was defined for the adhesive and one for the CFRP plies.

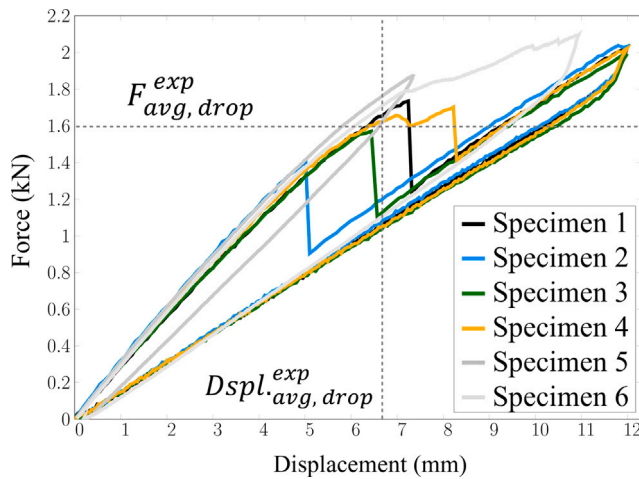


Fig. 4. Experimental force–displacement curves of the ENF specimens.

3. Results

3.1. Experimental data with optical analysis

Fig. 4 shows the force–displacement curves of the ENF tests. A total of six tests were performed where the response of the specimen 5 and 6 did not show an un-stable crack growth.

For the rest of the specimens, the load–displacement curves show a stepwise drop followed by a monotonic increase in force but softer response as the crack continues. This phenomenon defines instability of the crack initiation and it is associated with a discontinuity developing over the smooth surfaces [4]. The average peak load, $F_{avg, drop}^{exp}$, was used to calculate the G_{IIc} (G_{shc}) with an average experimental result of 6230 J/m^2 (by the ERR method [21]). The $F_{avg, drop}^{exp}$ of $1.6 \pm 0.15 \text{ kN}$ was determined at an average displacement, $D_{s_{pl}}^{exp, drop}$ of $6.7 \pm 1.34 \text{ mm}$.

Fig. 5-A shows the fracture surfaces along with the testing in the opened specimens. Multiple failure mechanisms took place during crack initiation.

The surfaces clearly demonstrate the mechanisms of adhesive failure (resin matrix) over an average length of 8 mm, occurring immediately beyond the pre-crack zone line. Adhesive remnants are visible on both adherends (Fig. 5-A). Furthermore, as illustrated in Fig. 12, the primary and dominant fracture mechanism took place within the bondline. Beyond the initial 8 mm length, the fracture surfaces exhibit CFRP on both sides, indicating a longitudinal failure at the 0° – 0° plies interface (refer to Fig. 5-B).

Fig. 6 shows detail images of the adhesive bondline at crack initiation point for the specimen 4 after the ENF test. It is important to mention that the specimen was cut in 45° with respect to the longitudinal direction, so that one cross-section shows actually a line from release film point to crack evolving towards other carrier (Fig. 6-A). This allows for a better representation of the carrier fibres (oval shape). The resin rich layer near adherends varies from 10–100 μm . At the middle of the two carriers, it can be also observed a resin rich region of about 100–300 μm .

3.2. Bondline fracture — simulated crack growth

The crack initiation was first simulated by the traditional VCCT and CZM methods at the bondline. These results enabled the calculation of fracture toughness, allowing for a direct comparison with experimental values. The models applied at the bondline, combined with the delamination implementation in the adherend using CZM, are collectively referred to in this study as the VCCT–CZM and CZM–CZM approaches.

The performance of both approaches in relation to the experimental load–displacement curves is presented in Fig. 7. Fig. 7-A focuses on the bondline failure using a single-method implementation (VCCT, CZM). Fig. 7-B highlights the prediction of delamination mechanisms within the adherend through the combined use of CZM with together VCCT or CZM approaches at the bondline.

The numerical results predict small force drops. The model with VCCT and CZM (for delamination) were able to demonstrate significant effects by the delamination on the specimen's response. For the model with only the CZM at the bondline, the use of reference values of material parameters does not lead to a fitting force drop. Higher values of the shear strength, τ_s^0 , were introduced to reach the value of the $F_{avg, drop}^{exp}$.

The CZM–CZM model with $\tau_s^0 = 120 \text{ MPa}$ responded with a reduced force drop effect when delamination was also predicted. This response might be due to 'softened' definition of penalty stiffness contact at the interfaces of the model.

3.3. Continuum damage models in simulations of ENF

3.3.1. Damage localization in ENF with single model

Fig. 8 presents the simulated force–displacement curves for the non-layered adhesive model (configuration M, as depicted in Fig. 3-A). The various curves shown in Fig. 8 correspond to the application of different material property values. The performance with reference properties resulted in an underestimation of the $F_{avg, drop}^{exp}$.

The variation of the strengths X_n , S_L and X_c were done in order to study their effects on the global response. Shear strength and compressive strength had an essential effect on the ENF response when normal strength (X_n) was kept constant. X_c was found to dominate the force drop response. Increases in X_c values resulted in a smoothing of the force response (removal of the drop). S_L had an effect on the peak and drop of the force. Higher S_L values decreased the force drop.

Fig. 9 illustrates the localization and damage evolution for the simulated models, referred to as Models A, D, and E. These models correspond to properties set defined by X_n values of 35, 90, and 200 MPa, respectively. The value of the strength X_n had a major effect on the localization and evolution of the damage. It can be observed that the model (i.e., Model 'a' in Fig. 8) accurately replicated the initiation pattern of the failure mechanism at the upper part of the adhesive, as observed in the experimental results.

The lower values of force predicted by the model with only CDM is probably due to high damage density promoting low structural stiffness in ENF when moduli starts to degrade.

3.3.2. The effects of elastic carrier layers in multi-layer models

The simulations of the multi-layer models are shown in Fig. 10. A range of values for shear and compressive strengths are run for the MCM (Fig. 10-A) and CMC (Fig. 10-B) layer configurations and compared with the experimental results.

The MCM model showed an underestimated force response where both shear and compressive strength value were too low. In simulations where only the S_L value was adjusted, the model predicted a force drop at $F_{avg, drop}^{exp}$. Increasing the value of X_c led to a minor reduction in the force drop. Moreover, the initial force drop was followed by a high density of normal damage (in a CDM layer), which contributed additional compliance to the ENF response.

The best matching force–displacement response was achieved by the CMC configuration when $S_L = 180 \text{ MPa}$ (CMC-III model). The high shear strength value did not bring only the expected damage response but also the largest force drop. A higher S_L value led to bigger drop and the continuation of finite elements to be totally damaged during the sliding step (see Fig. 11-b, folding). The predicted peak forces were essentially correct but occurred at lower displacements. The force–displacement response was not observably affected by the

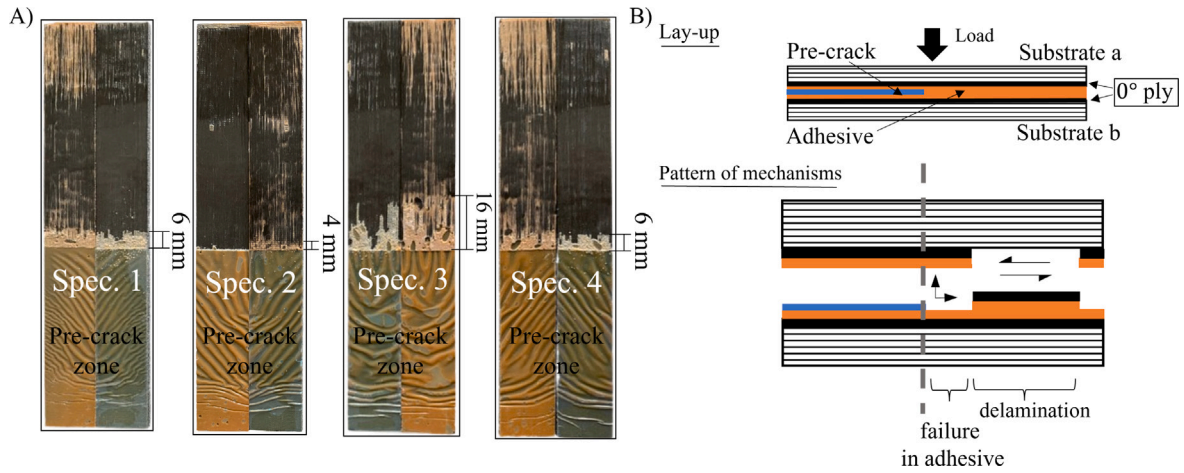


Fig. 5. (A) Fracture surfaces (xz-plane) of the opened specimens (post-test) and evaluated lengths of failure at bondline (in adhesive); (B) Change of failure mechanisms along the testing shown in 12-plane.

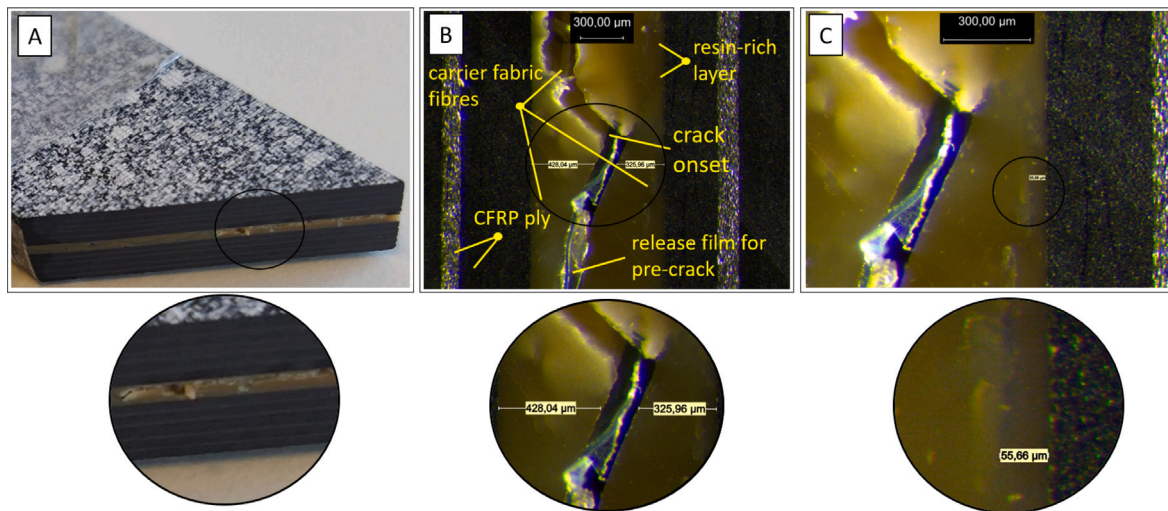


Fig. 6. Detail images of the adhesive bondline at the crack initiation point for the specimen 4 after testing: (A) 45° cut specimen 4 showing crack path at the bondline; (B) Microscopy image of the layered bondline at the crack initiation stage; (C) Microscopy image showing resin rich zone near the CFRP adherend.

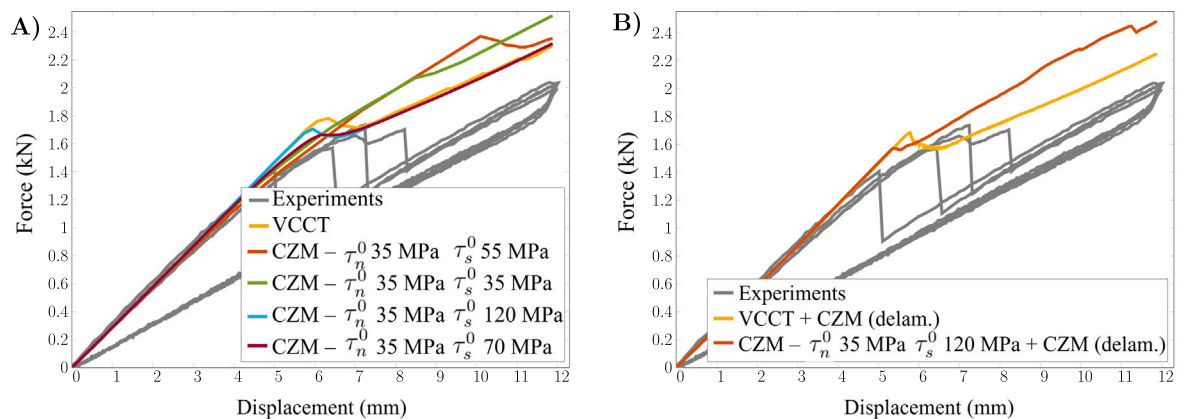


Fig. 7. Comparison of experimental load–displacement response with (A) single fracture model (VCCT, CZM) implementations at the adhesive bondline; (B) the VCCT–CZM and CZM–CZM implementations at the bondline and delamination (only CZM for delamination). Reference properties: $\tau_n^0 = 35$ (and 52) MPa $\tau_s^0 = 55$ (and 80) MPa $G_{Ic} = 1820$ (and 72) J/m² $G_{IIc} = 6230$ (and 779) J/m² (CZM for bondline and (ply–ply interface), respectively); $G_{Ic} = 1820$ J/m² $G_{IIc} = 6230$ (and 779) J/m² (VCCT for bondline).

crack modelling by CZM (CMC-III-CZM) at the interface failure of the adherends plies — this trend was observed for all values of S_L .

Fig. 11-A illustrates the location and extent of damage for each initiated failure mechanism in both the MCM and CMC configurations.

The degradation of stiffness in the adhesive modulus (via d_n) predominantly influenced the damage across the full thickness of the CDM layer and the initial F_{drop}^{num} . The degradation of shear modulus (d_{sh}) was the dominant factor at localized points along the bondline.

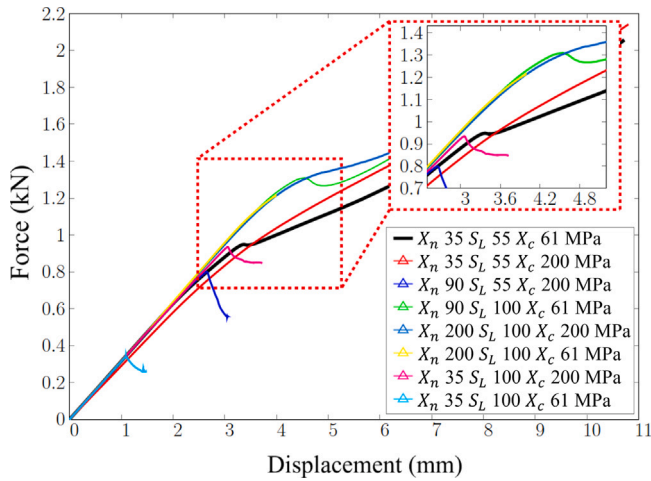


Fig. 8. Force–displacement curves for the ENF simulation with CDM with different strength values of film adhesive without layered modelling.

The CMC-III model's damage pattern was dominated by d_{sh} (shear modulus degradation) as shown in Fig. 11-B. Undamaged elements at the bottom CDM ("matrix phase") layer were able to carry load overcoming the force drop effect. Their degradation continued further only at higher force levels. The shear crack length of 6.48 mm, along the FEs of the (upper) bondline, was computed at the moment of the force drop. The CMC-III-CZM model predicted delamination failure along the adherend interface for $\tau_s^0 = 43$ MPa.

4. Discussion

4.1. ENF specimen and properties for (un-stable) crack initiation

The ratio of pre-crack length and span ($a/L \approx 0.5$) of the specimen in this study are out of the standard ENF testing [15]. Here, this ratio was used to investigate the un-stable crack initiation in the bonded ENF specimens. It is important to mention that numerous investigations have dealt with the sudden reversal shear and final fracture of diagonal ligaments for the ENF testing even with lower a/L ratios (within the standard values).

The current study presents the adhesive fracture toughness values originally determined at the crack initiation of DCB and ENF tests done with two FM 300-2 adhesive films and metallic adherends. The current, applied G_{Ic} (G_{nc}) falls between the determined range of 1600–2000 J/m² (averaged value throughout the crack propagation phase) [26]. The G_{IIc} (G_{shc}) value obtained in this study closely aligns with the results reported by Jokinen et al. [23]. The measurements [23] are in a typical range of adhesive films with similar fibrous carrier as the ones obtained for a 0.254 mm FM 300M adhesive [1]. The fracture toughness values fitted in this work are at the higher end of published values, even at the crack onset, as a consequence of the carrier structure type or number of adhesive plies bonded. The investigations with FM 300-2 adhesive but only one adhesive film ply presented a value of $G_{IIc} = 4897$ J/m² [23]. Works with different carrier type of FM 300 adhesives and by calculation with J-integral [33] resulted in lower (initial) fracture toughness values than the ones in this study.

The fracture toughnesses of CFRP interfaces in this study can be compared to the data obtained from a work of J.R. Reeder [34] related to AS4/3501-6 composite. By J.R. Reeder, $G_{Ic} = 81.6$ J/m² ($G_{IIc} = 554$ J/m², $\eta = 1.75$) was found by using the B–K criterion [35], and $G_{Ic} = 103$ J/m² ($G_{IIc} = 648$ J/m², $\alpha = 0.17$, $\beta = 4.8$) by using the Power law criterion [36]. In addition, it is important to mention that the results of damage modelling at the ply–ply interface mainly included the damage by shear component (and not normal component) when using the CMC-III-CZM model (see Fig. 11-b).

4.2. Experimental locus of the crack

The locus of crack initiation observed on the fracture surfaces, and based on the length of crack growth, has a direct correlation with the peak of the force drops in the load–displacement curves. Here, it can be seen that the maximum and minimum deviations are related to the lowest force peaks, while the cracks that had the 6 mm momentary length resulted in the highest force levels. These observations were properly modelled by the multi-layer CMC and MCM models. The use of the two layers of damageable matrix (i.e. the MCM model) were dominated by the d_n as damage cause and resulted in a lower force peak. The model with one matrix layer (i.e. the CMC model) was governed by the shear damage component predicting a crack tip locus of 6.48 mm when the force drop took place.

At the length scale of bondline, the experimental evidences of damage mechanisms have been reported by Jumel et al. [5] and Budzik et al. [2]. It was demonstrated that the origin of normal (opening) fracture in the adhesive is a consequence of unbalance of boundary conditions at the bondline due to softer regions during compressive stress loads far from the central loading zone.

Here, the ENF testing was coupled with DIC allowing measurement of the crack location and deformation of the specimen during test (See Section 2.1). Fig. 12-A shows DIC data and optical images of the fracture of the bondline at a maximum load and at force drop steps of the test.

The observations by the optical data demonstrate the initial trajectory of the crack towards the upper adhesive sheet. The mechanisms include a reversal shear damage (steps I–II), followed by the formation of diagonal microcracks (45°) in step III. This damage has a similar pattern than the epoxy interleaf failure between UD fibre reinforced laminates subjected to fracture Mode II in static loads investigated by Hojo et al. [18]. Finally, the fracture of the ligaments took place (step IV) causing the un-stable response indicated by the force drop. The fracture in the ligaments might have caused rotation as a consequence of transverse displacements to the normal direction, as suggested in the current literature [1].

Fig. 12-B, that includes DIC and simulated strain data, demonstrates that the onset of fracture occurs right at the border of the influence of the so-called Saint-Venant's principle of the effect of boundary [37]. The stiff adherends shield the crack tip effectively from the Saint-Venant's effects at the range of force used here. After crack initiation, the pin-boundary effect intensifies very rapidly. The shear response during the ENF test, however, is influenced by the central pin and the reversal of the shear direction at the midpoint of the three-point bending setup.

4.3. CDM applicability

It has been demonstrated in this study that the CDM can accurately reproduce failure mechanisms at the breadth of the bondline while predicting closely the load–displacement response. For that, geometrical and parametric analyses were carried out at the adhesive meso-structure and strength parameter S_L , respectively. The MCM and CMC layer-configurations cover potential situations of high or low damage accumulation along the thickness in the FPZ. From the modelling point of view, the carrier model could also be defined as a finite (penalty) stiffness at the bondline, [38], but with real geometry and property definition with certain directionality.

It is important to consider the enhanced Turon's constraint by Sarrado to relate the normal/shear ratio (τ_3^0/τ_{sh}^0) of strength values for the finite thickness adhesive [39,40]. Parametric studies subjected to the constraint have been reported in the literature with different τ_3^0/τ_{sh}^0 ratios in order to achieve close agreements with analytical or experimental curves of Mixed Mode Bending (MMB), DCB and ENF tests. In the current study, the observations show the involvement of damage mechanisms related to the normal direction from the joint

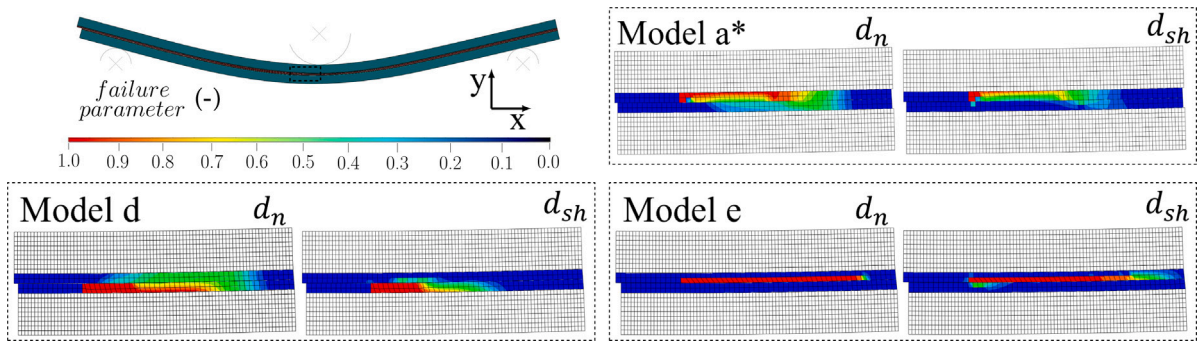


Fig. 9. Failure mechanisms for single adhesive Models A, D and E indicated by the nominal (d_n) and shear (d_{sh}) damage parameters at loading levels of $F^{num.} = 0.8, 1.2$ and 1.1 kN.

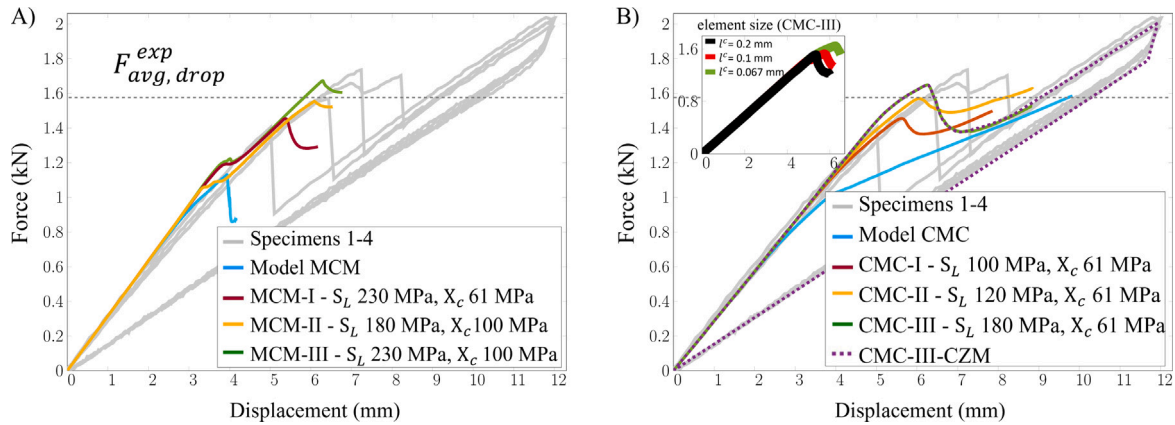


Fig. 10. Simulation of the ENF test for (A) the MCM and (B) CMC configurations, and ENF models with CZM applied for the longitudinal failure of the $0^\circ-0^\circ$ plies interface. Simulations run with property values: $X_n = 35$ MPa; $S_L = 55, 100, 120, 180, 230$ MPa; $X_c = 61, 100$ MPa; $G_{nc} = 1820$ J/m²; $G_{shc} = 6230$ J/m² (CDM). $\tau_n^0 = 55$ MPa; $\tau_s^0 = 55$ MPa; $G_{lc} = 1820$ J/m²; $G_{llc} = 6230$ J/m² (CZM).

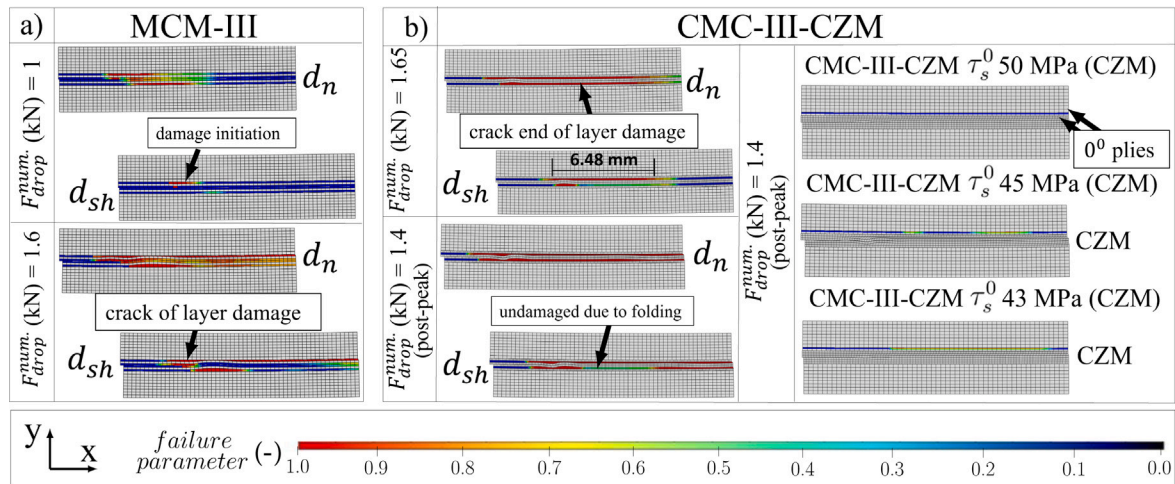


Fig. 11. Failure mechanisms performed as a result of stiffness degradations (d_n and d_{sh}) and damage in CZM: (a) MCM-III and (b) CMC-III and CMC-III-CZM.

plane. Here, it is suggested that parametric definitions and modelling of the adhesive structure are supported by the experimental evidences. This allowed for a correlation of the normal damage, d_n , with the formation of the diagonal micro-cracks at the upper adhesive, while the shear damage, d_{sh} (raise of S_L during sensitivity) tends to be dominant mechanism for the ligaments fracture up to the force drop.

The constitution of the CDM required a process of numerical-experimental analysis involving three parametric studies:

- Shear strength (τ_s^0) study to enhance CZM at the bondline, aiming to increase τ_s^0 for improved prediction of the force drops.
- Strength value study of single layered CDM, aiming to identify the influence of X_c and S_L on the force drop response. While X_c and S_L primarily govern the magnitude of the force drop, X_n plays a critical role in determining the failure location and the crack propagation path along the bondline.
- Strength value study of the multi-layer MCM and CMC models configurations to determine the d_{sh} parameter, aiming to

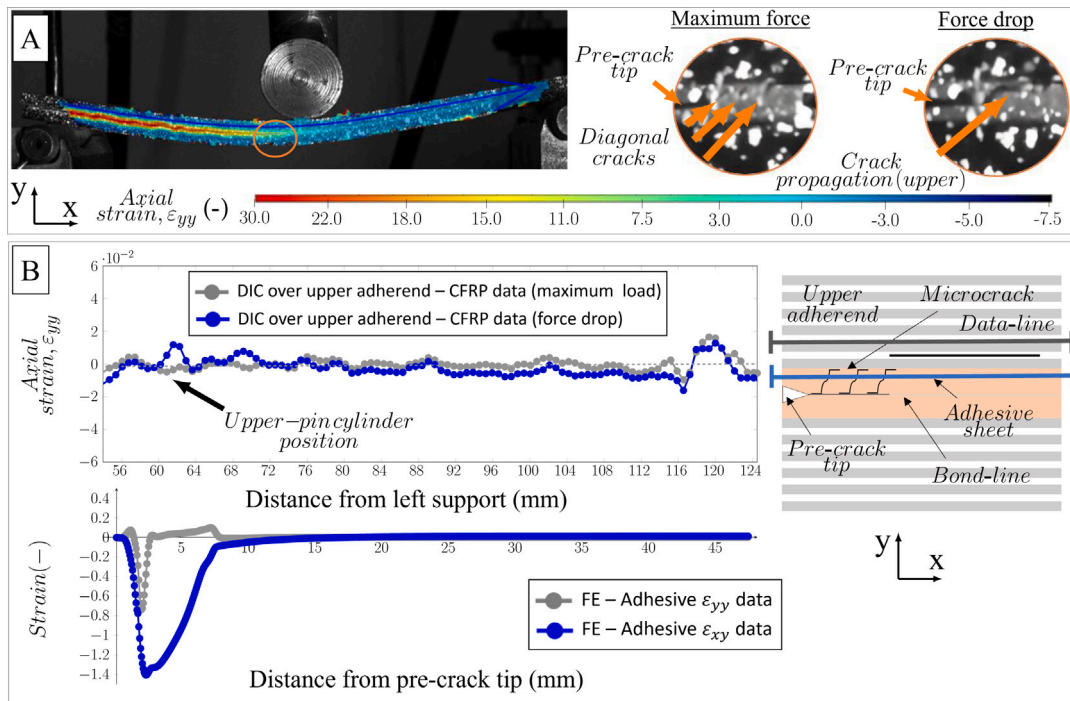


Fig. 12. (A) DIC data and optical images of the un-stable crack initiation in the adhesive bondline at a maximum load and at the force drop. The white markers represent the pattern used for data capturing for DIC. (B) Compressive out-of-plane deformation (strain in thickness direction by DIC and FE simulation by CMC-III model).

select the optimal meso-structure configuration for accurately predicting the onset of un-stable crack propagation.

The shear failure criterion defined in the constitutive model (Eq. 6) considers the material property subjected to thick adherend lap shear test. The modelling of the shear failure was in this work assumed as a brittle cleavage mechanism at the yielding point. This point was determined in the loading function (criterion) for shear with the standard thick adherend lap shear test (and data from KGR-1 extensometer from manufacturer's data [14]). The increase of the value for the S_L (or τ_v^0) in this study led to a low triaxiality pattern with corresponding potential to shear slip and therefore larger ductility, typical in the flexural ENF testing. Moreover, with S_L set to 180 MPa and the defined element (layer) thickness, the elastic energy in finite elements remained below the fracture toughness values in the CMC-III model [32].

The CMC-III model demonstrated the best prediction of the ENF (experimental) response with the initial pre-crack length of 68.5 mm. However, the un-stable crack propagation led to deviations in the experimental load–displacement responses, with a peak force scatter of approximately $\pm 10\%$. For that, simulations of the CMC-III model (pre-crack 68.5 mm) were run for G_{shc} values within a $\pm 25\%$ range variation to analyse the failure mechanisms at the FPZ. Results in Fig. 13 show a clear correlation between the magnitude of the force drop and the G_{shc} definition, as well as same crack propagation along the FPZ than the reference modelling. In addition, it is also illustrated the response of the CMC-III model for a shorter pre-crack length of 55 mm at the reference G_{shc} (6230 J/m^2). Regardless of the pre-crack length, crack propagation (direction, mode) was driven by the both damage parameters, d_{sh} and d_n , in similar way as depicted in Fig. 11-B. In the current literature, there are design of specimen that lead to stable Mode II fracture [8].

4.4. Stress triaxiality

The agreement of the CMC multi-layer configuration with respect to the experimental response is presumed to be related to the stress triaxiality at M (CDM) layers in the multi-layer modelling that provides a shear deformation between the adherends and “rigid body” rotation

of ENF locally. In large scale shear problems (e.g., lap-joint), large strain gradients due to substrates stiffness leads to a simple or non-simple shear condition [41,42]. For that, a triaxiality analysis is needed in order to determine the amount of hydrostatic stress and possible movement of flaws (e.g. micro void rotation), specially at the crack initiation where the force drop happens in the ENF specimens.

Fig. 14 shows the amount of hydrostatic pressure (p) and deviatoric stresses (\bar{s}) for the single and multi-layer configuration. The results are shown at the moment of the first localization damage (circle markers in Fig. 14-A.I and B.I) and prior to the force drop (triangle markers in Fig. 14-A.II and B.II).

During the elastic regime, both configurations show similar response with a high hydrostatic stress at the crack-tip (note that the simulations are all plane-strain states) with an increase of the \bar{s}_{12} for further distances ahead of crack tip. Towards the force drop (or significant change in force), the stress state presents a very low triaxiality.

The triaxiality of the multi-layer configuration exhibited an opposite behavior in terms of shear response (\bar{s}_{12}). This response is characterized by a continuous increase in \bar{s}_{12} up to the point of force drop. At this stage, the component equals the hydrostatic pressure at the crack tip, while its values remain non-zero beyond the crack tip. This behavior facilitates the storage of strain energy in shear, which provides sufficient energy to sustain the force increase following the drop phenomenon (as well as the kinetic energy transformation observed in real experiments) [4].

5. Conclusions

A new formulation based on CDM has been developed for finite thickness cohesive elements to accurately represent the un-stable crack initiation in adhesive films bonded to CFRP adherends subjected to the ENF testing. This development arose from experimental observations demonstrating the formation of a FPZ based on, besides shear damage mechanisms, normal transverse mechanisms with respect to the bondline causing. For that, a constitutive damage model was developed for the adhesive material. The model was based on the Bazant's crack theory accounting for initiation of the normal and shear failure. By

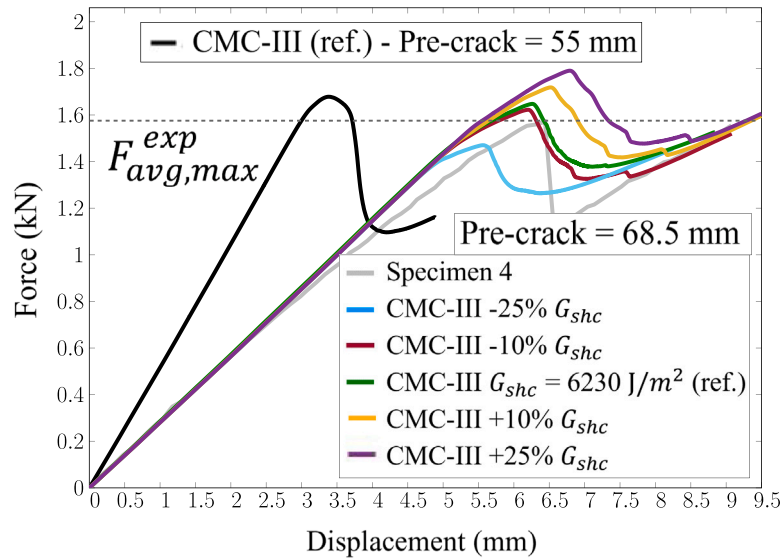


Fig. 13. Performance of the CDM-III model evaluated for two cases: (a) an initial pre-crack length of 55 mm with reference $G_{shc} = 6230 \text{ J/m}^2$, and (b) a variation of $\pm 25\%$ around the current G_{shc} fracture toughness with the reference pre-crack of 68.5 mm, corresponding to the existing pre-crack length.

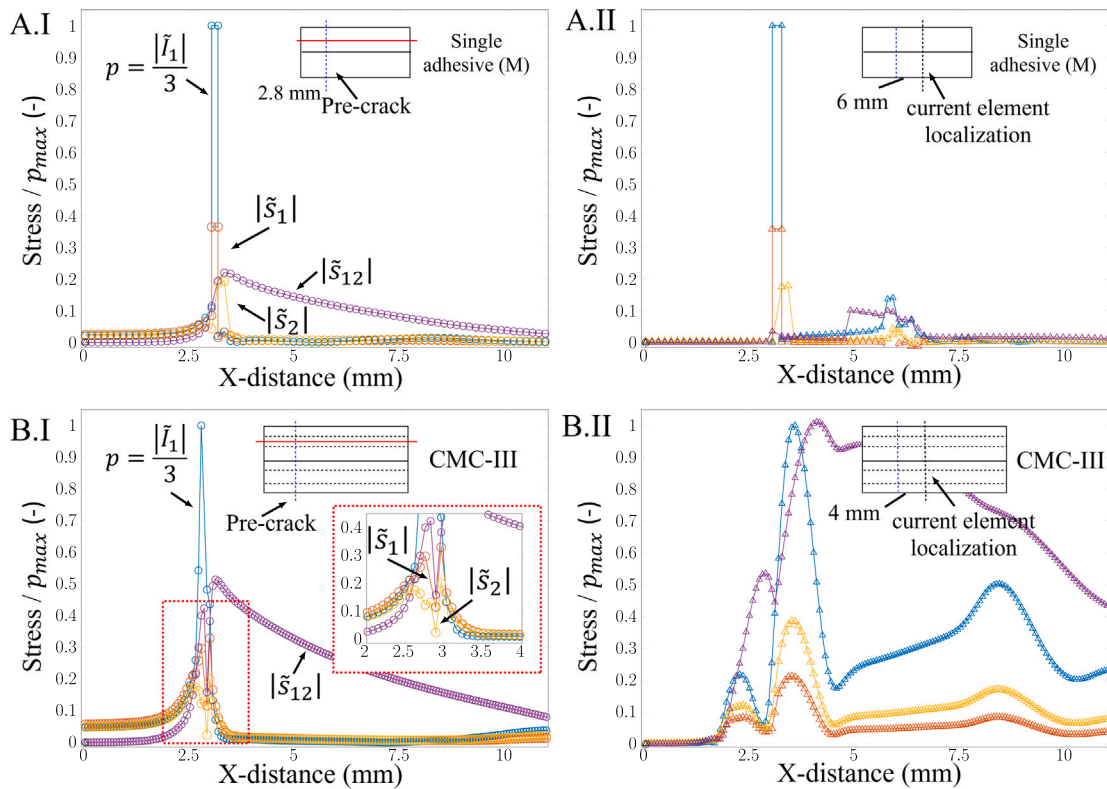


Fig. 14. Relative hydrostatic (p) and deviatoric stress state (\tilde{s}) for the single CDM model (A) and the CMC-III multi-layer model (B) at first damage localization (I) and prior the force drop (II). The results are shown for the upper (damaged) elements of the part representing the matrix phase (i.e. the M layer in multi-layer models).

means of a multi-layer representation of the adhesive meso-structure, proper dissipation of the matrix phase was performed among the elastic layers simplifying the effect of knitted carrier textiles inside the bondline. The simulations were complemented with the VCCT and CZM usage for comparisons and considerations of potential delamination in adherends.

Results have demonstrated the capability of the CDM to predict closely the force drop in the load–displacement curve of the ENF test. Different multi-layer configurations (MCM, CMC) were tested following

proper meso-structure definition of the adhesive thickness to model accurately the fracture process zone. Diagonal cracks at the bondline (previous to the force drop) served as experimental reference for the definition of the shear strength parameter of the adhesive model — solved iteratively with the rest of the damaged model properties fixed. The rise of the modelled shear strength allowed for keeping enough stored strain energy and leading to low triaxiality stress profile in the bondline typical in flexural response.

In addition, the use of VCCT and CZM for interlaminar delamination performed correctly to include the effects of multiple failure mechanisms in the ENF tests with composite adherends.

CRedit authorship contribution statement

O. Rodera: Writing – original draft, Visualization, Software, Methodology, Investigation, Formal analysis, Conceptualization. **N. Pournoori:** Writing – review & editing, Formal analysis, Data curation. **P. Hakala:** Data curation. **M. Kanerva:** Writing – review & editing, Validation, Supervision. **J. Jokinen:** Writing – review & editing, Validation, Supervision, Resources, Project administration, Funding acquisition.

Declaration of competing interest

The authors declare that they have no known competing financial interests or personal relationships that could have appeared to influence the work reported in this paper.

Acknowledgement

Unclassified. Based on Foreground information under European Defence Agency (EDA) Contract No B.PRJ.RT.670 covering the Ad Hoc Project entitled “PATCHBOND II”.

The work was supported by the (EDA) within the PATCHBOND II project (grant number B.PRJ.RT.670).

Appendix A. Compliance tensor

The compliance tensor is calculated as, $\mathbf{H}_m = \frac{\partial^2 \psi^{\varepsilon-d}}{\partial \sigma^2}$:

$$\mathbf{H}_m = \begin{pmatrix} \frac{1}{E_m(1-d_n)} & -\frac{\nu_m}{E_m} & -\frac{\nu_m}{E_m} & 0 & 0 & 0 \\ -\frac{\nu_m}{E_m} & \frac{1}{E_m(1-d_n)} & -\frac{\nu_m}{E_m} & 0 & 0 & 0 \\ -\frac{\nu_m}{E_m} & -\frac{\nu_m}{E_m} & \frac{1}{E_m(1-d_n)} & 0 & 0 & 0 \\ 0 & 0 & 0 & \frac{1}{G_m(1-d_{sh})} & 0 & 0 \\ 0 & 0 & 0 & 0 & \frac{1}{G_m(1-d_{sh})} & 0 \\ 0 & 0 & 0 & 0 & 0 & \frac{1}{G_m(1-d_{sh})} \end{pmatrix} \quad (\text{A.1})$$

where $G_m = \frac{E_m}{2(1+\nu_m)}$ is the shear modulus.

Appendix B. Determination of the tangent stiffness tensor, \mathbf{M}_m

The tensor \mathbf{M}_m from the general form of the tangent stiffness is defined as:

$$\mathbf{M}_{m,ij} = \frac{\partial H_{m,ij} \varepsilon_j}{\partial \varepsilon_k} = \varepsilon_j \frac{\partial H_{m,ij}}{\partial d_p} \frac{\partial d_p}{\partial r_\xi} \frac{\partial r_\xi}{\partial \varepsilon_k} \quad \text{with } i, j, k = \{1, 2, 3\} \quad \text{with} \\ \xi, p = \{1, 2\} \quad (\text{B.1})$$

where the sub-indices of the ξ and p refer to damage parameters d_n and d_{sh} . In addition, the convergence of the inelastic response was improved through a viscous regularization. Derivations of the regularization follow the form of Duvant–Lions [43].

Data availability

The data that has been used is confidential.

References

- [1] Leone FA, Girolamo D, Dávila CG. Progressive damage analysis of bonded composite joints. NASA/TM–2012-217790, 2012.
- [2] Budzik M, Jumel J, Ben Salem N, Shanahan M. Instrumented end notched flexure – crack propagation and process zone monitoring part II: Data reduction and experimental. Int J Solids Struct 2013;50(2):310–9.
- [3] Orell O, Jokinen J, Kanerva M. Use of DIC in the characterisation of mode II crack propagation in adhesive fatigue testing. Int. J. Adhes. Adhes. 2023;122:103332.
- [4] Carpinteri A, Paggi M. Analysis of snap-back instability due to end-Plane debonding in strengthened beams. J Eng Mech 2010;136(2):199–208.
- [5] Jumel J, Budzik M, Ben Salem N, Shanahan M. Instrumented end notched flexure – crack propagation and process zone monitoring. Part I: modelling and analysis. Int J Solids Struct 2013;50(2):297–309.
- [6] Sako R, Aoki R, Higuchi R, Ueda M, Urushiyama Y, Yokozeki T. Experiments on the mode II fracture toughness in ENF tests of CFRP curved beams. Compos Struct 2022;292:115692.
- [7] Leal A, Campilho R. Numerical evaluation of the ENF and 4ENF tests for the shear toughness estimation of adhesive joints. Compos Struct 2018;202:333–43.
- [8] Li X, Lubineau G. Towards stable end notched flexure (ENF) tests. J Mech Phys Solids 2024;192:105795.
- [9] Oshima S, Yoshimura A, Hirano Y, Ogasawara T, Tan K. In-situ observation of microscopic damage in adhesively bonded CFRP joints under mode I and mode II loading. Compos Struct 2019;227:111330.
- [10] Turon A, Camanho PP, Costa J, Dávila CG. A damage model for the simulation of delamination in advanced composites under variable-mode loading. Mech Mater 2006;38(11):1072–89.
- [11] Sarrado C, Leone FA, Turon A. Finite-thickness cohesive elements for modeling thick adhesives. Eng Fract Mech 2016;168:105–13.
- [12] de Moura MFSF, Chousal JAG. Cohesive and continuum damage models applied to fracture characterization of bonded joints. Int J Mech Sci 2006;48(5):493–503.
- [13] Rodera O, Jokinen J, Orell O, George L, Pournoori N, Kanerva M. Multi-layer continuum model for adhesive films with knitted carrier. Compos Sci Technol 2023;236:109981.
- [14] FM 300-2 film adhesive, technical data sheet. Cytec Engineered Materials; 2011.
- [15] D7905/D7905M-14 A. Standard test method for determination of the mode II interlaminar fracture toughness of unidirectional fiber-reinforced polymer matrix composites. Tech. rep., American Society for Testing and Materials; 2014.
- [16] Garde DB. Correspondence between adhesive joint strength, surface treatment and surface quality of cfrp (Master's thesis), Tampere University; 2023.
- [17] Schreier H, Orteu J, Sutton MA. Image correlation for shape, motion and deformation measurements. Springer US; 2009.
- [18] Hojo M, Ando T, Tanaka M, Adachi T, Ochiai S, Endo Y. Modes I and II interlaminar fracture toughness and fatigue delamination of CF/epoxy laminates with self-same epoxy interleaf. Int J Fatigue 2006;28:1154–65.
- [19] Skytta V, Saarela O, Wallin M. Progressive failure of composite laminates 564-analysis vs experiments. In: Gdoutos EE, editor. Fracture of nano and engineering materials and structures. Dordrecht: Springer; 2006.
- [20] Altair Engineering. Altair engineering inc. eSAComp (2017). Material database. ESAComp; 2019.
- [21] Jokinen J, Orell O, Wallin M, Kanerva M. A concept for defining the mixed-mode behaviour of tough epoxy film adhesives by single specimen design. J Adhes Sci Technol 2020;34(18):1982–99.
- [22] Jokinen J, Kanerva M, Wallin M, Saarela O. The simulation of a double cantilever beam test using the virtual crack closure technique with the cohesive zone modelling. Int. J. Adhes. Adhes. 2019;88:50–8.
- [23] Jokinen J, Wallin M, Kanerva M. The influence of the number of adhesive plies (FM 300-2) on fracture properties. In: The 32nd congress of the international council of the aeronautical sciences. 2020.
- [24] Jokinen J, Wallin M, Kanerva M, Saarela O. Analyses of criticality for multiple site delaminations in the flap spar of finnish f/a-18 aircraft. Aeronaut. J. 2020;125:556–77.
- [25] Rybicki EF, Kanninen MF. A finite element calculation of stress intensity factors by a modified crack closure integral. Eng Fract Mech 1977;9(4):931–8.
- [26] Jokinen J, Wallin M, Saarela O. Applicability of VCCT in mode I loading of yielding adhesively bonded joints – a case study. Int. J. Adhes. Adhes. 2015;62:85–91.
- [27] Dassault Systèmes. abaqus 2017 documentation, user's manual. 2017.
- [28] Maimi P, Camanho PP, Mayugo JA, Davila CG. A thermodynamically consistent damage model for advanced composites. NASA/TM-2006-214282, Hampton, VA; 2006.
- [29] Melro AR, Camanho PP, Andrade Pires FM, Pinho ST. Micromechanical analysis of polymer composites reinforced by unidirectional fibres: part I - constitutive modelling. Int J Solids Struct 2013;50(5):1897–905.
- [30] Tschögl NW. Failure surfaces in principal stress space. J Polym Sci Polym Symp 2007;32(1):239–67.
- [31] Sun CT, Chen JL. A simple flow rule for characterizing nonlinear behavior of fibre composites. J Compos Mater 1989;23(10):1009–20.

- [32] Bažant ZP, Oh BH. Crack band theory for fracture of concrete. *Mater Struct* 1983;(16):155–77.
- [33] Sarrado C, Turon A, Costa J, Renart J. On the validity of linear elastic fracture mechanics methods to measure the fracture toughness of adhesive joints. *Int J Solids Struct* 2016;81:110–6.
- [34] Reeder JR. 3D mixed-mode delamination fracture criteria – an experimentalist's perspective. In: 21st annual technical conference of the american society for composites. Dearborn, MI; 2006.
- [35] Benzeggagh M, Kenane M. Measurement of mixed-mode delamination fracture toughness of unidirectional glass/epoxy composites with mixed-mode bending apparatus. *Compos Sci Technol* 1996;56(4):439–49. [http://dx.doi.org/10.1016/0266-3538\(96\)00005-x](http://dx.doi.org/10.1016/0266-3538(96)00005-x).
- [36] Whitcomb JD. Analysis of instability-related growth of a through-width delamination. NASA TM-86301, 1984.
- [37] Rizzoni R, Dumont S, Lebon F, Sacco E. Higher order adhesive effects in composite beams. *Eur J Mech A Solids* 2021;85:104108.
- [38] Camanho PP, Davila CG, de Moura MF. Numerical simulation of mixed-Mode progressive delamination in composite materials. *J Compos Mater* 2003;37(16):1415–38.
- [39] Turon A, Camanho P, Costa J, Renart J. Accurate simulation of delamination growth under mixed-mode loading using cohesive elements: Definition of interlaminar strengths and elastic stiffness. *Compos Struct* 2010;92(8):1857–64. <http://dx.doi.org/10.1016/j.compstruct.2010.01.012>.
- [40] Sarrado C, Turon A, Renart J, Urresti I. Assessment of energy dissipation during mixed-mode delamination growth using cohesive zone models. *Composites A* 2012;43(11):2128–36. <http://dx.doi.org/10.1016/j.compositesa.2012.07.009>.
- [41] Nielsen KL. Ductile damage development in friction stir welded aluminum joints (AA2024). *Eng Fract Mech* 2008;75(10):2795–811.
- [42] Kanerva M, Besharat Z, Pärnänen T, Jokinen J, Honkanen M, Sarlin E, Göthelid M, Schlenzka D. Miniature CoCr laser welds under cyclic shear: fatigue evolution and crack growth. *J Mech Behav Biomed Mater* 2019;99:93–103.
- [43] Łapczyk I, Hurtado JA. Progressive damage modeling in fiber-reinforced materials. *Composites A* 2007;38(11):2333–41.